Improved visual inspection for nozzle inner radius based on panoramic imaging

Sanao Huang, Ke Xu, Ruixin Wang
Collaborative Innovation Center of Steel Technology
University of Science and Technology Beijing
Beijing, China

Maocheng Hong
CGN Inspection Technology Co., Ltd
Suzhou, China

Abstract— **Visual inspections of Nuclear Power Plant (NPP) reactors are important for understanding the current condition of the reactor components, such as nozzle inner radius. After addressing current deficiencies of the existing visual inspection methods, a panoramic image mosaicking method is proposed in this study to improve the efficiency and reliability of detection. However, unlike traditional mosaicking methods, the proposed method obtains the variation of the pixels between frames in a video by establishing a geometric mapping relationship between scenes and images. Then, the pixels which are varied between frames will be extracted and the frames will be combined to generate the mosaicked images. A function to discriminate overexposed pixels is also derived based on the redundant pixels in a series of frames, to reduce the impact of specular reflection on the resulting images. These above methods are applied to the detection of defects on nozzle inner radius of the mock-up. The resulting 360° panoramic images provide a large-field-of-view defect analysis approach to obtaining geometric measurements with pixel-level precision, and the image optimization method is found to mitigate the effects of specular reflection on defect identification by providing clear and reliable images. The results of this study demonstrate the promise of this new visual inspection method for NPP reactors, and establishes a potential foundation for the automatic detection of surface defects.**

Contribution—**A method is presented to improve the reliability of defect detection, and it has been applied to the visual inspection for nozzle inner radius.**

Keywords—Visual inspection; Reactor pressure vessel; Nozzle inner radius; Panoramic image; Image mosaicking; Specular highlight removal

I. INTRODUCTION

Over extended periods of time, there are many various factors, such as high radiation and stress concentrations, affect the surfaces of key NPP components detrimentally. Surface defects which are likely to occur in the primary loop materials, such as cracks, exhibit accelerated growth under these factors, leading to severe degradation [1]. These defects and associated damages must be effectively detected on the inner surfaces of the key components of NPPs in their early stages, to prevent loss of containment and disaster.

Visual inspection is the main method for detecting defects, structural integrity issues, or leakage traces on the surface of key components in an NPP. Recent technological developments have considerably improved the accuracy and efficiency of visual inspection methods. The demands for more advanced visual inspection techniques is increasing. For example, cracks on nozzle inner radius of reactor pressure vessel (RPV) have been identified using this method. Due to the structure of nozzle inner radius, it is difficult to perform a volume defect detection method such as ultrasonic inspection, and the obtained results are typically unsatisfactory. The American Society of Mechanical Engineers (ASME) standards stipulate that enhanced visual inspection can be used as a replacement for volume defect detection to detect small incidences of damage, identify the type of damage, and quantify the severity of damage [2].

Existing visual inspection methods rely on a single-frame image analysis to identify defects. However, it is difficult to locate manually, image, and measure defects [3]. Occasionally, the lack of full-scale observations makes it difficult to evaluate certain parameters, such as the potential size of the defect. Moreover, some inspection tasks can only be performed using frozen and magnified images, where patterns of surface defects may only appear as insignificant changes. Finally, the inspection environment is harsh and the surfaces are monotonous in coloration, which can lead to the errors of identifying defects.

Machine vision and image processing technology have been widely used in industrial non-destructive testing. For example, during the production of metal plates, surface inspection systems based on machine vision technology enable the manufacturers to detect, track, and grade surface defects. Companies such as Cognex in the US, NKK in Japan, and Parsytec in Germany have been actively developing such devices, which can effectively detect different types of defects online. Tang et al. designed a pipeline defect detection system achieving defect detection and identification automatically [4]. Owing to these advances, there is potential to improve efficiency and help resolve the insufficiency of the current detection technology in the field of nuclear power. Machine vision technology has been applied to fuel assembly deformation measurements [5]. Obviously, such techniques will be beneficial for a wide range of applications in nuclear power field. However, their applications in the field of nuclear power are still limited.

Large field-of-view images, such as panoramic images, can be used to improve the reliability of visual analysis methods and defect detection. Tang et al. used an active stereo omni-directional vision sensor to provide a 360° panoramic

978-1-7281-9331-1/20/$31.00 ©2020 IEEE

inspection for internal pipe defects [4]. However, this sensor cannot operate without the additional equipment. Another method for obtaining 360° imagery is designing an image mosaicking algorithm to merge multiple images into a single panoramic image by overlapping areas, to form a larger scene. However, most traditional image mosaicking methods use feature detection to merge and overlap images [6,7], but the target surfaces of NPP components notably lack features, which makes it difficult to apply these methods. An image mosaicking method for a high-temperature gas-cooled reactor core has been proposed; however, this method has limitations, as successful mosaicking was only achieved for specific objects, and the pixel variation between frames in the videos could not be addressed, implying that the accuracy of this method cannot be guaranteed [8]. An accurate measurement of the dimensions of the defects in the panoramic image for visual inspection is provided in [9]. However, it requires objects of known size, such as keyways and brick heights to calculate scaling factors. It is not suitable for visual inspection if there is no opportunity to find any object of this kind. To the authors' knowledge, 360° image inspection has not been applied to the detection of defects on nozzle inner radius of an RPV. Accordingly, this study derives and employs an image mosaicking method using a conventional NPP visual inspection device to create panoramic images to detect and measure defects on nozzle inner radius from inspection videos.

A notable challenge in any image-based visual inspection is the presence of specular highlights, especially on metal surfaces, it will result in overexposed pixels in the images. The presence of specular highlights can hide small defects in the images causing them to be missed during inspection. A number of methods have been proposed to separate or remove specular reflection: using more than one image [10], and using only one image [11]. Most solutions involved the complicated non-linear optimization [12,13]. An averaging method to remove specularity from data is presented in [14], using to image-based dietary assessment. However, since it relies on averaging, features in the final result can appear blurred and distorted. Multiple image methods suggested in previous works require special capturing apparatus or only apply to color images [10]. An approach which exploits additional information in neighboring frames from video footage to reduce specularity from each frame is presented in [12]. However, this approach requires a pre-processing method in which image correspondence is performed using the Scale-Invariant Feature Transform (SIFT) algorithm. It is not suitable for visual inspection where a lack of surface features limits the application of this method. However, in this study, the information of overlapping frames from video data, which depict the same point in multiple frames, are utilized to optimize the images by using pixel values from other frames to replace overexposed pixels. This practical method for effectively reducing overexposure in inspection images can enhance detection reliability.

This study proposes two complementary methods to improve the visual inspection of NPP components. Using the proposed mosaicking method, the size information of defects can be more effectively extracted from a panoramic image, and enable more accurate measurements of surface defects. Furthermore, the proposed specular highlight removal method can make defect identification easier and more reliable. In this paper, Section II provides the background and overview of a visual inspection system for nozzle inner radius. Section III describes the algorithm details for the proposed image mosaicking method using captured video frames, and the specular highlight removal method applied together for creating the panoramic images alongside the proposed method for image-based defect measurement. Section IV demonstrates the capabilities of the proposed methods in a complex structure by using them to detect defects on nozzle inner radius of an RPV; the experimental setup and the detection results are also discussed in this section. Section V presents the conclusions of this study.

II. Detection of Defects on Nozzle Inner Radius of an RPV

This study focuses on the detection of defects on inner radius of the inlet and outlet RPV nozzles. In the HPR1000 reactor, the diameters of the inlet and outlet nozzles are both 760 mm. Fig. 1 depicts the inlet nozzle on the upper, with a 6° inclination close to the shell, and the outlet nozzle on the lower. The body material of this nozzle is 16MND5 steel, and the inner wall has a 7-mm thick layer of 309L and 308L austenitic stainless steel. The inspection zones on the inner radius of the RPV nozzles, determined according to the requirements specified in ASME Code, are also indicated in Fig. 1.

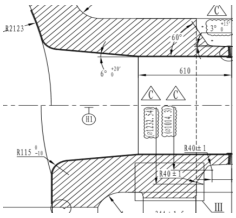

(a)

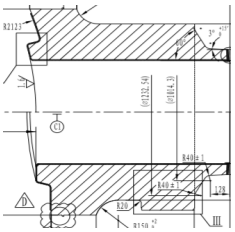

(b)

Fig. 1 Inspection zones on the inner radius of RPV nozzles

The defects that must be identified include: 1) mechanical damage, such as scratches and impacts; 2) cracks and arc strikes; and 3) corrosion locations. In addition to these defects, the proposed method of providing images for surface defect detection should enable reliable identification of minor defects with a sensitivity satisfying the requirements of VT-1 [2]. Moreover, the defects may need to be evaluated both qualitatively and quantitatively.

A. Inspection System Overview

An independent video inspection system for nozzle inner radius surfaces of an RPV is comprised of a remotely operated vehicle (ROV), motion device, positioning device, and video

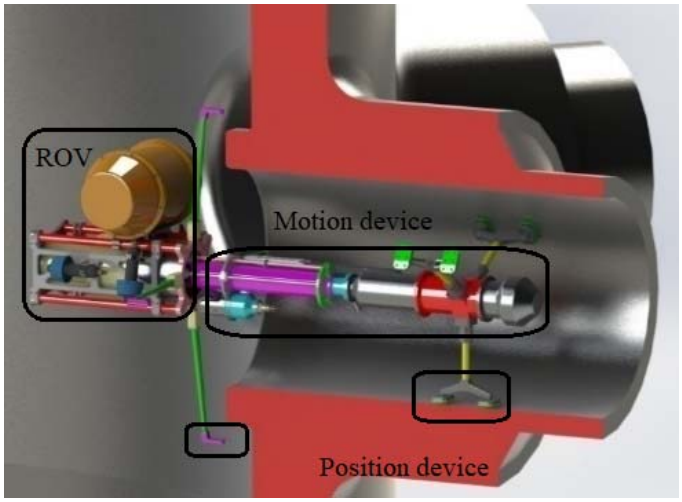

Fig. 2 Inspection system for the inner radius of RPV nozzles

capture system. The ROV platform is equipped with several propellers to facilitate floating, diving, forward and backward motions, and course changing. Moreover, the integrated level gauge and gyroscope can be used to generate balanced torque to maintain stability. After the motion device and ROV enter the nozzle, the positioning device is used to locate the system inside the nozzle, as shown in Fig. 2. The motion device has two degrees: rotation around the nozzle axis and translation along the nozzle axis.

An underwater pan/tilt/zoom (PTZ) unit is used as the video capture system. It consists of a camera recording at 60 fps with a resolution of 1920 x 1080, a number of light sources, and a built-in pan-tilt device. The pan and tilt functions allow adjustment of the camera's angle of view. The PTZ camera was attached to the motion device and could rotate 360° about the axis of the nozzle to record videos for the target zone.

B. Existing Image Capture and Data Analysis Method

The inspection system is used to position the cameras facing the surface within a field limited to the zone under examination. Thus data can be recorded by scanning the internal surface. Data analysis is performed by inspectors; therefore, suitable frames are required for observation and evaluation to make a qualified evaluation. As the existing analysis method is based on single-frame image, it is often difficult to evaluate defects due to the lack of full-scale observations and difficult to evaluate certain parameters, such as the potential size of the defect. Thus, some inspection tasks cannot be solved using existing analysis methods.

III. Proposed Panaromic Imaging Methods

A. Image Mosaicking Method

An image mosaicking method is proposed to assemble the individual frames from a video into a 360° panorama. The mapping relationship between image pixels and their corresponding scene points determines the pixel's position, size and brightness.

Defining the center of the camera lens O_C as the origin of the coordinate system, the *Z*-axis is the line passing through the optical center and perpendicular to the image plane, and $P\left(x_i, y_i, z_0\right)$ is the scene point mapped to pixel $I\left(x_i^{'}, y_i^{'}, f^{'}\right)$. Then,

$$x_i = x_i^{'} \cdot \frac{z_0}{f^{'}} \text{ and } y_i = y_i^{'} \cdot \frac{z_0}{f^{'}} \tag{1}$$

where $f^{'}$ is the current focal length [15]. However, because both $f^{'}$ and z_0 are independent variables and unknown, it is difficult to obtain the mapping coordinates of a scene using Equation (1).

Assuming that two points in a scene, $P_1\left(x_1, y_1, z_1\right)$ and $P_2\left(x_2, y_2, z_2\right)$, are mapped to pixels $I_1\left(x_1^{'}, y_1^{'}, f^{'}\right)$ and $I_2\left(x_2^{'}, y_2^{'}, f^{'}\right)$, respectively in an image, then, from Equation (1),

$$\frac{\| P_1 - P_2 \|}{\| I_1 - I_2 \|} = \frac{z_0}{f^{'}} + \xi(\Delta z_1, \Delta z_2) \tag{2}$$

where $\|\cdot\|$ represents the length of the vector between points or pixels; Δz_1 and Δz_2 represent $|z_0 - z_1|$ and $|z_0 - z_2|$, respectively; and $\xi(\Delta z_1, \Delta z_2)$ is a quadratic polynomial function. When the values of the two independent variables are both 0, the value of this function is 0.

During the inspection, the camera's angle of view is assumed to be perpendicular to the target surface. When the angle of view and distance remain basically unchanged during inspection, the geometric relationships between the coordinate systems of the camera, the image, and the scene are as illustrated in Fig. 3, in which the X_C, Y_C, and Z_C represent the coordinate system of the camera. Considering the center of the camera lens O_C as the origin and the line passing through the optical center and perpendicular to the image plane as the *Z*-axis, the camera plane, image plane, and target surface can all be considered approximately parallel to each other [16].

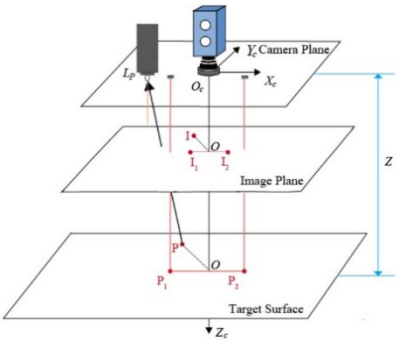

Fig. 3 Schematic of inspection for surface defects

As under these conditions the depth of the scene changes negligibly compared to the distance between the camera and the surface of the scene, *Z* is almost constant and is equal to the distance between the surface of the scene and the plane upon which the optical center of the camera resides. Thus, the assumption of orthographic projection can be adopted instead of a perspective projection [15]. Moreover, the value of the quadratic polynomial function in Equation (2) is approximately 0. Then, $z_0 / f^{'}$ can be determined by solving the ratio on the left-hand side of Equation (2) to obtain the coordinates of the points mapped in the scene.

Thus, a two-stage process is designed:

1) The value of $z_0 / f^{'}$ is determined via using two lasers;
2) A formula to calculate the pixel variation between frames is established, containing the inspection parameters.

Any two reference points separated by a known distance can be used to solve the ratio on the left-hand side of Equation (2). By equipping the inspection device with two laser generators fixed at *d*, were the distance between the two laser lines in the image is *D*, then,

$$\frac{z_0}{f^{'}} \approx \frac{\| P_1 - P_2 \|}{\| I_1 - I_2 \|} = \frac{d}{D} \tag{3}$$

Therefore, the scene point $P\left(x_i, y_i, z_0\right)$, which is mapped to pixel $I\left(x_i^{'}, y_i^{'}, f^{'}\right)$ in the image, is obtained as follows:

$$x_i = x_i^{'} \cdot \frac{d}{D} \text{ and } y_i = y_i^{'} \cdot \frac{d}{D} \tag{4}$$

Equation (4) determines only the mapping relationship between the pixel and the scene point. The pixel size parameter is defined as follows:

$$h = \frac{d}{D} \tag{5}$$

If the distance between the laser lines is fixed at 22 mm, and supposing that the distance between the two parallel laser lines is measured to be 275 pixels in the image, the pixel parameter *h* can be calculated as follows: 22 mm ÷ 275 px = 0.08 mm / px, indicating that each pixel is 0.08 mm in size.

During the defect inspection of nozzle inner radius surface of an RPV, the actual number of different pixels between any two frames in the video can be expressed as follows:

$$k = \frac{v \cdot \Delta t}{60 \cdot h} \tag{6}$$

where *v* denotes the inspection speed (in mm/s) and Δt denotes the time difference between two frames (in seconds). If the camera speed *v* is constant, the different pixels between frames at any fixed time interval also remains constant. Therefore, images with this number of pixels can be extracted at fixed frame intervals from the video, and these images can be mosaicked into a complete image based on the inspection speed.

By establishing the mapping relationship between the scene and the image, the patterns of pixel variations between frames of the video and the pixel difference values that should be extracted can be accurately calculated. To prevent subpixel differences, the appropriate inspection speed *v* can be calculated using Equation (6), and an integer value of pixel difference *k* can be obtained by selecting the appropriate time interval Δt, ensuring an accurately mosaicked image.

B. Image Optimization Method

In order to remove specular highlights, a method is proposed to replace overexposed pixels using multiple frames from the video. The frame size in the video is *W*×*H* and the number of pixels to be extracted for image mosaicking is *k*. Then the size of the patch extracted from a single frame is *k*×*H*. Meanwhile, the scene captured in the patch is mapped to *W*/*k* frames theoretically.

As the goal is to produce visually pleasing images, a first attempt is to reduce the overexposed pixels. Calculating the number of pixels whose grayscale values exceed the threshold p in the patch firstly.

Also, the average grayscale value of pixels in the patch *P* has an impact on the quality of the panoramic image, thus it is calculated as follows:

$$\overline{f} = \frac{1}{N} \sum_{p \in P} f\left(p\right) \tag{7}$$

where *N* is the number of pixels *p* in the patch, and $f\left(p\right)$ is the grayscale value of the pixel.

To capture the best characteristics of both, we propose to combine them:

$$E = \alpha \cdot \frac{\overline{f}}{255} + \left(1\text{-}\alpha\right) \cdot \frac{m}{N} \tag{8}$$

where there are *m* pixels in the patch whose grayscale values exceed the threshold. The Equation (8) is simply the

weighed sum of its two terms. We empirically set α=0.15. We did not perform a thorough investigation although we tested a few different values.

Subsequently, the values of E are calculated and the patch with the smallest one is selected to replace the overexposed one.

C. Defect Measurement Method

According to Equation (3), the distance between any two points on the target surface can be calculated as follows:

$$\| P_1 - P_2 \| = \| I_1 - I_2 \| \cdot \frac{d}{D} \quad (9)$$

The theoretical precision of the measurements obtained using Equation (9) is at the pixel level. When reviewing the processed images to identify surface defects, the containing image, position, and size of each defect should be recorded. The length of linear defects should be measured, whereas for planar defects, both length and width should be measured.

IV. Experimental Evaluation

A. Evaluation Method

This study evaluated the proposed image processing methods for improving the detection of surface defects on the inner radius of RPV nozzles using a mock-up, modeled in Fig.4, with similar dimensions to an actual RPV nozzle.

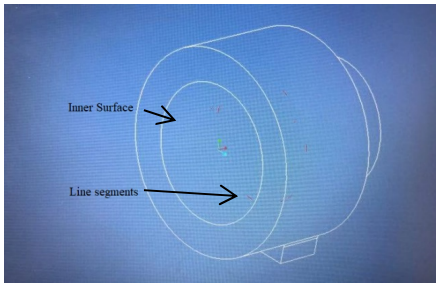

Fig. 4 Simulation and video scan of the RPV nozzle mock-up

In these experiments, eight line-segments of different lengths and directions were drawn inside the nozzle mock-up, to simulate defects at different circumferential positions in the nozzle region. The length of each line segment was measured three times using a measuring tape, and the lengths reported in Table 1 are the averages of these three measurements. The actual lengths of the test line segments shown in Table 1 were then compared to the lengths measured using the mosaicked and processed images to determine the accuracy possible when using the proposed image processing methods. Then, further experiments were conducted to verify the compatibility and reliability of the proposed 360° image mosaicking method based on the accuracy of defect measurements taken using different inspection and camera parameters.

TABLE I. Actual Lengths of Test Line Segments

Nozzle Line Segment No.	***Length, Z1 (mm)***	***Nozzle Line Segment No***	***Length, Z1 (mm)***
1	50.1	5	20.1
2	20.0	6	49.9
3	50.1	7	49.4
4	49.9	8	18.7

B. Initial Results

First, to demonstrate the efficacy of the proposed image mosaicking and specular highlight removal methods, a 360° video was recorded and processed. The mosaicking result obtained for the nozzle section from the video at a zoom value of 2.0 and an inspection speed of 1.6° per second is shown in Fig. 5. The upper image shows the panoramic image generated according to the method detailed in Section 2.1, whereas the lower images show specific zones after specular highlight removal, as described in Section 2.2. Figs. 6(a) to 5(f) show locally magnified images of the eight defects and their measured lengths.

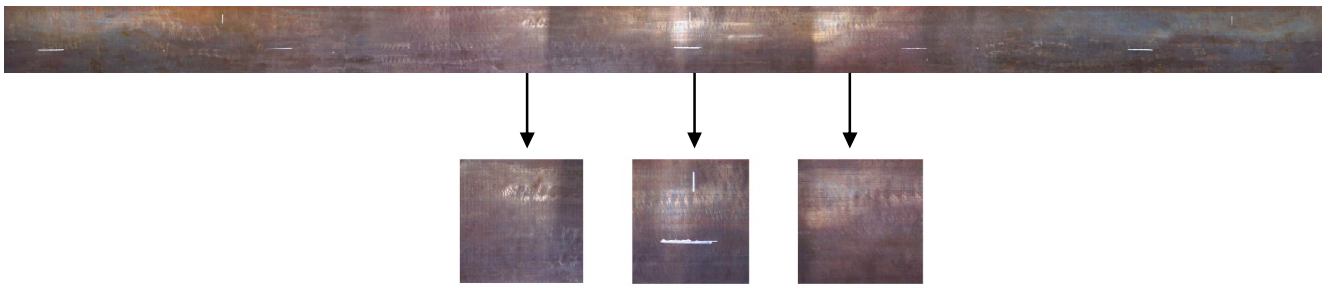

Fig. 5 Mosaicked image and specific zones after specular highlight removal.

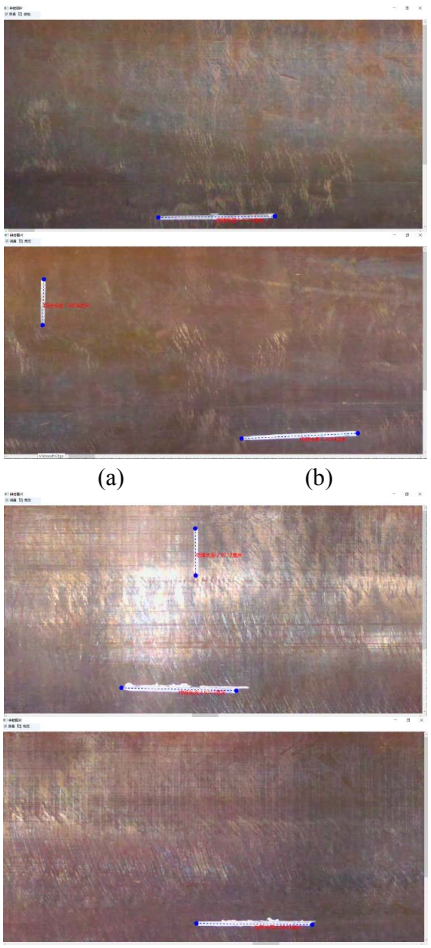

(a) (b) (c) (d)

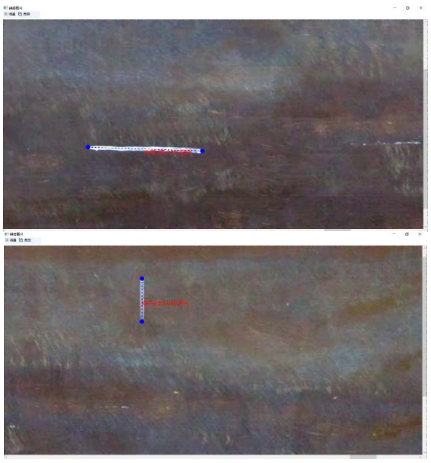

(e) (f)

Fig. 6 Defect analysis from visual inspection of the inner radial surface of the mock-up RPV nozzle (Units: cm)

The results show that the proposed method is very useful and can provide quite reliable visual inspections using currently available devices. From Fig. 5, the appearances of defects in the generated panoramic images are complete and clear, with unambiguous positions and sizes. Image optimization has effectively reduced the impact of specular overexposure, improving the reliability of defect detection from the images.

Unlike recent methods [8,9], which assume a value for the variation of the pixels between frames, we calculate them by calibrating pixel sizes. It is clear that the proposed method can produce more reliable mosaicking image. Moreover, it enables the accuracy can be guaranteed even with different inspection parameters or camera patterns. In this test, if we extract 5 pixels per frame like [8], there is a big deviation with the actual sizes.

Once the panoramic image has been generated, more detailed observations and measurements can be conducted using the local magnification function to improve the identification of small defects. For the locally magnified photos of the eight defects shown in Figs. 6(a) to 6(f), the information shown is clear, and the measured sizes are close to the actual sizes, as shown in Table 2:

TABLE II. MEASURED SIZES OF TEST LINE SEGMENTS

Nozzle Line Segment No.	*Length, Z1 (mm)*	*Errors (mm)*	*Nozzle Line Segment No*	*Length, Z1 (mm)*	*Errors (mm)*
1	50.3	0.2	5	20.2	0.1
2	19.8	-0.2	6	49.8	-0.1
3	50.3	0.2	7	49.2	-0.2
4	49.7	-0.2	8	18.5	-0.2

It is important to note several limitations of the current study:

Firstly, it was assumed that the camera's angle of view was perpendicular to the target surface and both the angle of view and distance remained basically unchanged during the inspection; this may not be the case in all potential applications.

Additionally, the assumption of orthographic projection adopted in the current study may cause errors for image modeling. Therefore, for specific scene P_j, the patches extracted from the edges do not necessarily correspond to those from the center. Accordingly, it is more reasonable to place a limit on the patches without causing a large distortion in this application.

C. Evaluation of Different Inspection Parameters

According to Equation (6), the extracted pixel difference between frames is related to the inspection parameters, therefore when the pixel difference is not an integer, there will be errors in the mosaicked image. Therefore, to test the impact of inspection speed on measurement accuracy, three different inspection speeds, 1.8°/s, 2.4°/s and 2.5°/s were evaluated at a zoom value of 1.0. The length of each defect line segment was then measured in the resulting mosaicked images, and the

relative errors between the measured and actual lengths were calculated with the results shown in Fig. 7.

The first two inspection speeds, 1.8°/s and 2.4°/s, were appropriate to be calculated using Equation (6), obtaining an integer value of pixel difference k by selecting the appropriate time interval Δt. Therefore, the defect measurements collected were found to match the actual lengths. However, the defect measurements collected at the third inspection speed, 2.5°/s, deviated from the actual lengths as the speed input into the calculation resulted in subpixel differences. Indeed, when the inspection speeds used in the proposed mosaicking calculation did not cause subpixel difference, the image-measured length of each line segment was very close to the actual value with relative errors within a range of -0.20–1.00%. Otherwise, the range of relative errors increased to 2.00–6.00%. This indicates that the presence of subpixel differences undermines the accuracy of the mosaicking results and thus decreases the image-based measurement precision. Additionally, these results suggest that different inspection speeds, when accurately applied in the proposed image mosaicking method, have only a slight impact on the accuracy of the measurements taken from the images.

D. Evaluation of Different Camera Patterns

According to Eq. (6), the extracted pixel difference between frames is also related to the pixel parameter, which depends on the zoom value of the camera. Therefore, videos were recorded at three inspection speeds, 2.4°/s, 2.0°/s and 1.6°/s, calculated as specified in Section III.A. and the frames were subjected to image mosaicking at zoom values of 1.0, 1.5, and 2.0 to provide the same value of k for each image. The length of each defect line segment was then measured in the processed images with the resulting measurement errors shown in Fig. 8.

These results demonstrate that under all three camera parameters, there was no evident difference between the actual values or any of the obtained lengths. This indicates that irrespective of how the camera parameters are set, accurate 360° images and relatively high measurement precision can be obtained using the proposed method.

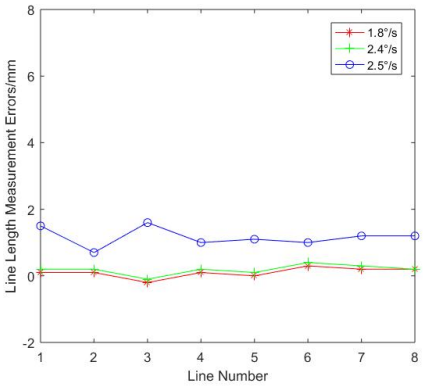

Fig. 7 Measurement errors with different inspection parameters

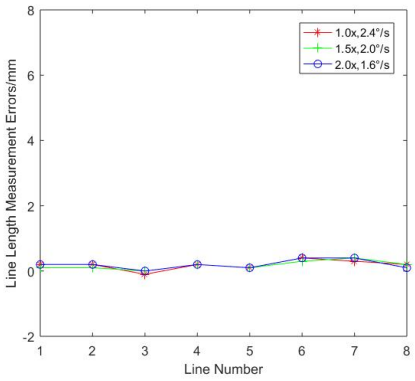

Fig. 8 Measurement errors under different camera parameters

V. CONCLUSIONS

In this study, image mosaicking and optimization methods for producing high-quality 360° panoramic images from video information are proposed and verified by analysis and experiments. The proposed methods are developed to provide large-field-of-view images for defect detection and overcome the problems associated with the single-frame methods, such as highly subjective and difficulties in defect identification. Using the proposed methods, defects were identified and accurately measured under a variety of inspection and camera parameters. The proposed methods can therefore be applied to reduce the risk of missing defects effectively and improve the reliability.

The application of the proposed mosaicking and specular highlight removal methods to the visual inspection of nozzle inner radius will allow for more accurate and reliable inspections. However, there are several limitations, such as the assumption that the camera's angle of view is perpendicular to the target surface as well as the fixed angle of view and distance to the inspected object, which limit the application of the proposed methods in more complex inspection tasks. In future, we will determine the parameters of such complex tasks and evaluate their impacts on the efficacy of the proposed methods through further experimentation. Additionally, remove the instances of specular highlights that are present in all frames of the video inspection and thus not addressed by the proposed method could further improve the clarity of the processed image. Moreover, the conversion from video data to static images presenting in this study may establish a promising foundation for the automatic detection of surface defects. It is, however, important to note that the potential improvement provided by the proposed methods can only be fully realized if both the software and hardware used in inspections are also improved. As it is expected that new market applications will continue to emerge as the benefits of this more reliable approach are investigated, this research may also be relevant to the design of improved inspection devices for future generations of NPP reactors and other limited-access, condition-critical infrastructure.

REFERENCES

[1] S. Cumblidge, S. Doctor, and M. Anderson. "The Capabilities and Limitations of Remote Visual Methods to Detect Service-Induced Cracks in Reactor Components," ASME Pressure Vessels and Piping Conference, Volume 5: High Pressure Technology, Nondestructive Evaluation, Pipeline Systems. Vancoucer, BC, Canada: ASME, 2006:183-193.

[2] NRC Regulatory Guide 1.147: In-service Inspection Code Case Acceptability. ASME Section XI, Division 1, Revision 16 [S].

[3] T. Ertl, A. Romanova, S.Tait , and K. Horoshenkov. "Sewer inspection and comparison of acoustic and CCTV methods," In Proceedings of the *ICE-Water Management*, 2013; 166(2):70-80.

[4] Y.P. Tang, T. Wu, G.P. Yuan, S.H. Lu and Z.Y. Yang. "3D Omni-directional vision sensor for morphology defects detection in pipelines," Chinese Journal of Scientific Instrument, 2017, 38(3): 726-733.

[5] J. Arias and W. Hummel. "Fuel Services Progress in Visual Examination and Measurements on Fuel Assemblies and Associated Core Components Track 1," In Proceedings of *Top Fuel 2009*; 2009 Sept 6-10; Paris, France.

[6] G. Debabrata and K. Naima. "A survey on image mosaicking techniques,"J VIS COMMUN IMAGE R. 2016; 34:1-11.

[7] Y.S. Chen and Y.Y. Chuang. "Natural Image Stitching with the Global Similarity Prior," In Proceedings of *ECCV 2016*, Part V, pp. 186-201, October 2016, Amsterdam, Netherland.

[8] P. Murray, G. West, S. Marshall, andS. McArthur. "Automated in-core image generation from video to aid visual inspection of nuclear power plant cores,"NUCL ENG DES. 2016; 300:57-66.

[9] M. Devereux, P. Murray, and G. West. "Automated Analysis of AGR Fuel Channel Inspection Videos" Poster session presented at *2019 Innovation Showcase: Nuclear Asset Management and Industrial Informatics*. Toronto, Canada. May 2019.

[10] S.Iwata, K.Ogata, and S. Sakaino. "Specular Reflection Removal with High-Speed Camera for Video Imaging" In Proceedings of *IECON 2015*, pp. 1735-1740.

[11] Y. Liu, Z. Yuan, N. Zheng, , and Y. Wu. "Saturation-Preserving Specular Reflection Separation," In Proceedings of *CVPR 2015*, pp. 3725-3733.

[12] S.M.Z.A. Shah, S. Marshall, and P. Murray. "Removal of specular reflections from image sequences using feature correspondences," MACH VISION APPL," 2017; 28:409-420.

[13] Q.X. Yang, J.H. Tang, and N. Ahuja. "Efficient and Robust Specular Highlight Removal,"IEEE T PATTERN ANAL. 2015; 37(6):1304-1311.

[14] Y. He, , N. Khanna, , C.J. Boushey, , and E.J. Delp. "Specular Highlight Removal for Image-Based Dietary Assessment," In Proceedings of *ICMEW 2012*, pp. 424-428.

[15] B.K.P. Horn. Robot Vision [M]. Cambridge: The MIT Press, 2014.

[16] S. Huang, K. Xu, M. Li and M. Wu. "Improved Visual Inspection Through 3D Image Reconstruction of Defects Based on the Photometric Stereo Technique," Sensors. 2019, 19(22): 4970.